Raman scattering studies in dilute magnetic semiconductor $Zn_{1-x}Co_xO$

K. Samanta, P. Bhattacharya, and R. S. Katiyar
Department of Physics, University of Puerto Rico, San Juan, Puerto Rico 00931-3343

W. Iwamoto, P. G. Pagliuso, and C. Rettori
Instituto de Fisica DEQ-UNICAMP Cidade Universitaria- Barao Geraldo 13083-970 Campinas, SP, Brazil
(Received 13 February 2006; revised manuscript received 14 April 2006; published 26 June 2006)

Raman spectra of ZnO and Co substituted $Zn_{1-x}Co_xO$ (ZCO) were carried out using the Raman microprobe system with an Ar^+ ion laser source of 514.5 nm wavelength. The shift towards the lower frequency side of the nonpolar E_2^{low} mode and the broadening due to Co substitution in ZnO were analyzed using the phonon confinement model. The magnetic measurements showed ferromagnetic behavior with the maximum saturation magnetization ($1.2\mu_B$/Co) for 10% Co substitution, which decreased with at further increase in Co concentrations. The intensities of E_1(LO) at 584 cm^{-1} and multiphonon modes at 540 cm^{-1} were increased with an increase in Co substitution. The additional Raman modes in ceramic targets of ZCO spectra for higher concentration of Co substitution ($x=15\%-20\%$) were identified to be due to the spinel $ZnCo_2O_4$ secondary phase.

DOI: 10.1103/PhysRevB.73.245213 PACS number(s): 75.50.Pp, 78.30.Am, 78.66.Hf

INTRODUCTION

Zinc oxide (ZnO) is a direct band gap II-VI compound semiconductor with the wurtzite-type structure. Its high (3.37 eV) band gap energy and large excitonic binding energy (60 meV) at room temperature, makes it a potential candidate for ultraviolet (UV) optoelectronic devices such as light emitting diodes, laser, and photodetectors.[1–4] Recently, ZnO alloying with the 3*d* transition metal (TM) has attracted much attention as a dilute magnetic semiconductor (DMS), with room temperature ferromagnetism, for spintronic applications.[5,6] In the host wurtzite ZnO, the isovalent transition metals (Co^{2+}, Mn^{2+}, Ni^{2+}, etc.) are the substitutes at the Zn cation sites. The coupling of localized *d* electrons of the TM with the host semiconducting band gap leads to a number of exciting properties such as magneto-optical and magneto-electrical effects.[7–9] The ferromagnetic transition temperature (T_c) in dilute magnetic semiconductor increases due to the increase in *p-d* hybridization and a reduction of spin-orbit coupling.[10]

There are several theoretical arguments as well as experimental reports that predict that $Zn_{1-x}Co_xO$ may be the most promising DMS material for room temperature ferromagnetism.[11,12] However, the major drawbacks with the experimental reports are often the parameter windows that are very narrow with a poor reproducibility. For instance, recent controversial reports[13] reveal that the ferromagnetism in $Zn_{1-x}Co_xO$ is not an inherent property but because of the segregated secondary phases or clustering related to Co, Co_3O_4 and the isomorphic $Zn_xCo_{3-x}O_4$. Nondestructive characterizations such as Raman and infrared spectroscopy are extensively used to study the substitution in the host lattice and identify the impurity phases. Moreover, vibrational spectroscopy is crucial for constraining the lattice dynamical model, to understanding thermodynamical properties, and for constraining phase equilibrium.[14] Thus, to recognize the fundamentalism of the thermal as well as electrical properties, it is essential to know the vibrational modes of the crystal. Also one of the most important aspects of substitutional semiconductor alloys is the nature of the alloy potential fluctuation (APF),[15] which have been extensively studied in III-V and II-VI ternary alloy semiconductors.[16–19] Nonetheless, according to our knowledge, no detail Raman investigation of Co substituted ZnO have been reported yet. In this paper, we, therefore, use micro-Raman spectroscopy to study the effects of Co substitution on the lattice dynamical properties of ZnO in light of the phonon confinement model. We also carried out magnetic measurements of these samples and correlated it with the lattice dynamical properties. For comparison, we also studied $ZnCo_2O_4$ assuming Co_3O_4 and its isomeric compounds including $Zn_xCo_{3-x}O_4$ as the most probable impurity phase.

EXPERIMENTS

The ceramic targets of $Zn_{1-x}Co_xO$ ($x=0-0.2$) and $ZnCo_2O_4$ for pulsed laser deposition were prepared by conventional ceramic processing using ZnO and Co_3O_4 powders. An excimer laser (KrF, 248 nm, 10 Hz) with the laser energy of 2.5 J/cm^2 was used to deposit the films on Al_2O_3 (0001) substrates. The deposition chamber was evacuated to $\sim 10^{-6}$ Torr background pressure. The substrate temperature was maintained at 650 °C. Oxygen was introduced by keeping the pressure at 1 mTorr. The target to substrate distance was maintained at 5 cm and the deposition period was 17 min. The thickness of the films grown was ~800 nm. The crystal structure and the phase formation of ZnO and $Zn_{1-x}Co_xO$ ceramics and thin films were characterized with the x-ray diffraction technique using the Siemens D5000 x-ray diffractometer (XRD) with Cu $K\alpha$ radiation. The optical transmission spectra were recorded using the UV-VIS spectrometer (Perkin Elmer model RS-2) in the range of 300–800 nm. The micro-Raman measurements were performed in the backscattering geometry using the Jobin-Yvon T64000 Triple-mate instrument. The radiation of 514.5 nm from a coherent argon ion laser was focused to ~2 μm in

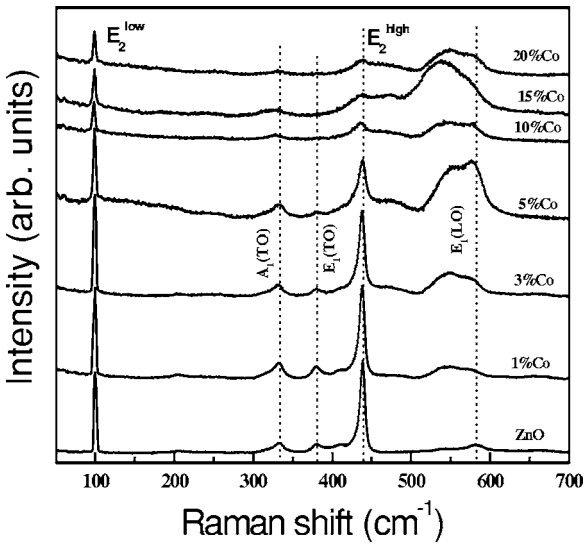

FIG. 1. Room temperature Raman spectra of $Zn_{1-x}Co_xO$ targets for different x (0–0.2) values.

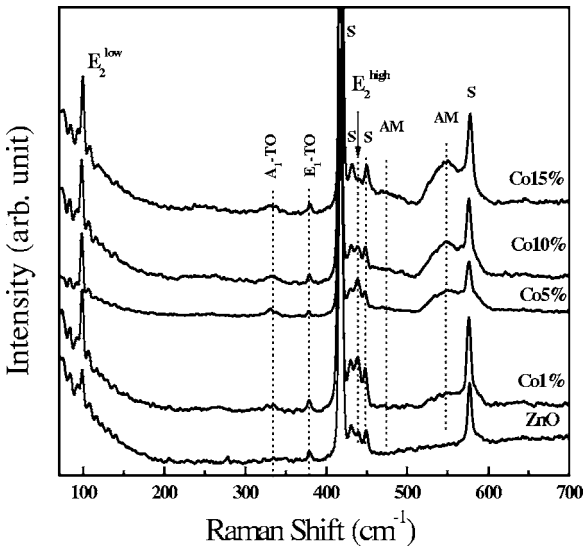

FIG. 2. Room temperature Raman spectra of $Zn_{1-x}Co_xO$ thin films for different x (0–0.15) values on Al_2O_3 substrates (s).

diameter on the samples. A LN_2 cooled charge-coupled device (CCD) system was used to collect and process the scattered data. Magnetic measurements were carried out in a Quantum Design MPMS SQUID magnetometer between 2 and 300 K and −1.5 and +1.5 T.

RESULT AND DISCUSSION

Our XRD results showed there is no secondary phase in $Zn_{1-x}Co_xO$ (ZCO) within the detection limit of the measurement.[20] However, micro-Raman spectra of $Zn_{1-x}Co_xO$ ceramic targets and thin films at room temperature revealed that there are several additional features due to Co substitution (Fig. 1). The E_2^{low} peak position of ZnO was shifted towards the lower frequency (up to 10% Co) and there was an increase in FWHM for up to 10% of Co substituted ZnO; the FWHM nearly saturated on the further increase (15% and 20%) of Co concentration. The broad band centered at 540 cm^{-1} and an additional mode at 470 cm^{-1} in ceramic targets is observed due to Co substitution (Fig. 1).

The wurtzite structure of ZnO has the space group C_{6v}^4 with two formula units per primitive cell with all atoms occupying C_{3v} sites. Each Zn atom is tetrahedrally coordinated to four O atoms and vice versa. The numbers of optical symmetry modes for the C_{6v}^4 are given by

$$\Gamma = A_1(z,z^2,x^2+y^2) + 2B_1 + E_1(x,y,xz,yz) + 2E_2(x^2-y^2,xy).$$

The B_1 modes are silent in Raman scattering where A_1 and E_1 modes are polar and hence, exhibit different frequencies for the transverse-optical (TO) and longitudinal-optical (LO) phonons, because of the macroscopic electric field associated with the LO phonons. The nonpolar E_2 modes have two frequencies, namely, E_2^{high} and E_2^{low} associated with the motion of oxygen (O) atoms and zinc (Zn) sublattice, respectively.[21]

The first order Raman modes for ZnO and Co substituted ZnO ceramic pallets (used for thin film deposition) are shown in Fig. 1. We observed five normal modes at 99.8, 333, 379, 437.7, and 584 cm^{-1} corresponding to E_2^{low}, $A_1(TO)$, $E_1(TO)$, E_2^{high}, and $E_1(LO)$, respectively, with intense E_2^{high} and E_2^{low} modes. The E_2^{low} peak position of ZnO shifted towards the lower frequency by $\sim$1.30 cm^{-1} in samples with 10% Co and the FWHM increases with an increase of Co substitution. The backscattering Raman spectra for highly c axis oriented ZCO thin films clearly show (Fig. 2) E_2^{high} and E_2^{low} modes besides the strong modes of Al_2O_3 substrates. The E_2^{low} peak position of ZnO shifted towards the lower frequency side similar to targets by $\sim$0.90 cm^{-1} at 10% Co substitution in ZnO. The atomic substitution in a host lattice induces structural disorder. This disorder breaks the translational symmetry of the allowed phonons of the host lattice and leading to the contribution of $q \neq 0$ phonons to the Raman line shape, corresponding to the finite size effect. The disorder-induced effects (lower frequency shift and broadening) in $Zn_{1-x}Co_xO$ can be explained by alloy potential fluctuations (APF) using a spatial correlation (SC) model.[15] In an ideal crystal the region over which the spatial correlation function of the phonon extends is infinity. When the crystal is alloying, the spatial correlation region of the phonon becomes finite owing to the potential fluctuation of the alloying disorder, which gives rise to the relaxation of the $q=0$ selection rule in Raman scattering.

The assumption of a Gaussian attenuation factor $\exp(-2r^2/L^2)$, where L is the diameter of the correlation region, leads to an average over q with a similar weighting factor $\exp(-q^2L^2/4)$ upon Fourier transformation. It was successfully used to account for the **q** vector relaxation related to the finite size effect[22] and the structural disorder.[23] We assume a finite spatial correlation region in the alloying material and then the Raman intensity at a frequency ω can be written as,[15]

$$I(\omega) \cong \int_0^1 \frac{4\pi q^2 \exp(-q^2L^2/4)dq}{[\omega-\omega(q)]^2 + [\Gamma_0/2]^2}, \quad (1)$$

where q has the unit of $2\pi/a$, a is the lattice constant, Γ_0 (=3.66 cm^{-1}) is the FWHM of E_2^{low} mode of the undoped

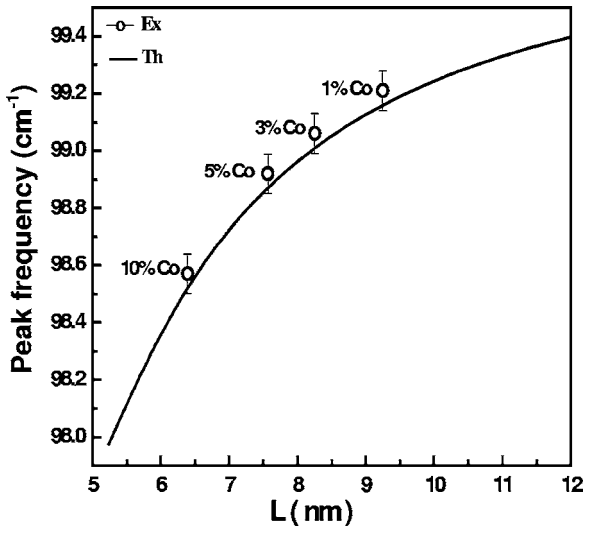

FIG. 3. Plot of correlation length (L) vs Raman peak frequency for E_2^{low} modes of $Zn_{1-x}Co_xO$ targets for different x values. The solid line represents the theoretical values using Eqs. (1) and (2).

ZnO Raman line. Assuming at one-dimensional linear chain model, the dispersion relation for the wurtzite ZnO structure can be written as follows by assuming the analytical mode relationship:

$$\omega(q) = A + B\cos(\pi q), \tag{2}$$

where $A=73.8$ cm^{-1} and $B=26$ cm^{-1} for the E_2^{low} phonon dispersion according to the *ab initio* phonon dispersion relation calculated for ZnO.[24] Considering the correlation length, L, as an adjustable parameter we get the value of L by fitting the Raman line shape of the E_2^{low} band. The estimated L values corresponding to 1%, 3%, 5%, and 10% Co doped ZnO are 9.248, 8.253, 7.565, and 6.391 nm, respectively. Figure 3 shows that the E_2^{low} phonon peak shifts to the lower frequency side as the correlation length decreases; the agreement in both experimental and theoretical cases is quite good. The FWHM of E_2^{low} phonon of $Zn_{1-x}Co_xO$ is shown in Fig. 4. The FWHM increases with an increase in Co concentration up to 10%, from 3.66 to 5.85 cm^{-1} and nearly saturate for further increases of Co concentration.

The additional Raman modes at 204 cm^{-1} and 542 cm^{-1} were detected in ZCO ceramic spectra as the second order multiphonon modes. It is interesting to note that with the increase of Co concentrations up to 20%, the intensity of the multiphonon mode at 540 cm^{-1} and E_1(LO) at 584 cm^{-1}, are increased substantially. In thin film spectra a broad shoulder around 548 cm^{-1} is clearly evident in Co substitutions (Fig. 2). A similar increase in the intensity of the multiphonon band in the range of 500–600 cm^{-1} was also reported for P^+ implanted ZnO, which was attributed to the defect induced band. They have also shown that after annealing the intensity of this multiphonon mode was reduced. Manjon *et al.*[25] claimed that the Raman modes around 580 cm^{-1} correspond to the B_1 (high) silent mode of wurtzite ZnO using *ab initio* calculations. This mode can be observed in disorder activated Raman scattering due to relaxation of the Raman selection rules produced by the breakdown of the transnational

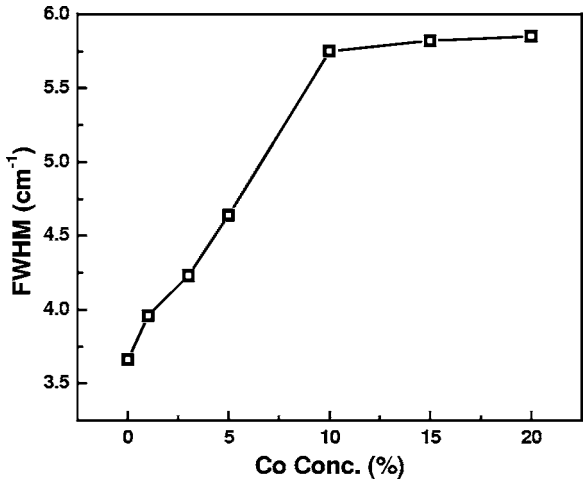

FIG. 4. Full width at half maxima of E_2^{low} modes of $Zn_{1-x}Co_xO$ targets for different Co concentration.

symmetry. We try to explain this increase of E_1(LO), besides defects, as due to the resonant Raman effect at sub-band-gap absorption related to *d-d* transition of Co in ZCO. The optical absorption spectra ZCO clearly show a strong absorption band in the sub-band-gap (2.2–3.0 eV) region related to the *d-d* crystal field splitting and the charge transfer absorptions as shown in Fig. 5. The Raman excitation source, Ar^+ laser, has an energy of 2.4 eV (514.5 nm), which is above some of the sub-band-gap states.

Several recent results have been reported on anomalous Raman modes in doped and alloyed ZnO bulk and thin films grown by different techniques.[26,27] To understand the additional modes (AM) due to Co substitution we have also studied $ZnCo_2O_4$ bulk and thin films on Al_2O_3 substrates. The possible secondary phases in Co substituted ZnO are Co clusters, Co_3O_4, and/or its isomeric compound $Zn_xCo_{3-x}O_4$ as mentioned earlier. A comparison of Raman spectra for 15% Co doped ZnO and $ZnCo_2O_4$ ceramic targets are presented in Fig. 6. In the case of ceramic targets, for $Zn_{1-x}Co_xO$ we are able to identify additional modes mainly

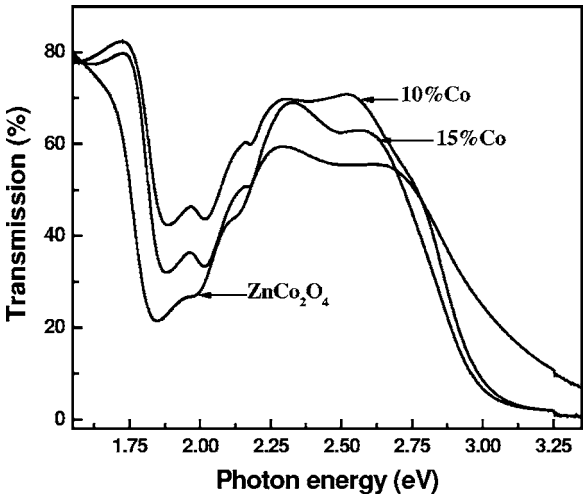

FIG. 5. Optical transmission spectra of $Zn_{1-x}Co_xO$ ($x=0.1, 0.15$) and $ZnCo_2O_4$ thin films on Al_2O_3 substrates.

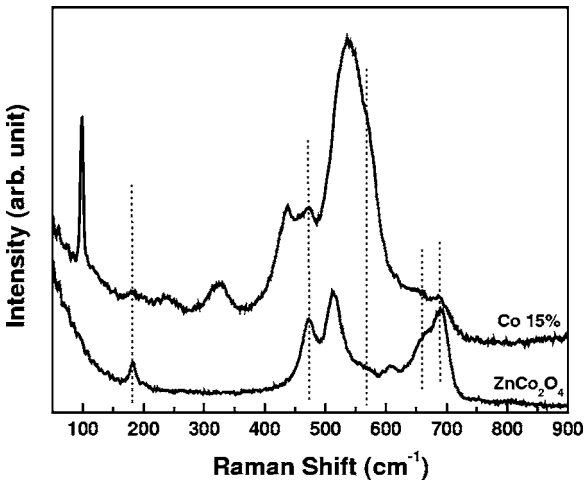

FIG. 6. Comparison of Raman spectra for $ZnCo_2O_4$ and $Zn_{0.85}Co_{0.15}O$ targets.

due to $ZnCo_2O_4$, however for thin films, we are unable to identify any mode of these secondary phases.

We have carried out the magnetic measurements (M vs H) on $Zn_{1-x}Co_xO$ thin films, and these are shown in Figs. 7 and 8. The saturation magnetization for 3%, 5%, and 10% Co substituted ZnO was observed as 0.11, 0.24, and 1.2 μ_B/Co, respectively. It is evident from these data that 10% of the Co substitution produces the maximum saturation magnetic moment (1.2 μ_B/Co), and the Ms value was found to decrease for 15% and 20% Co substitution (Fig. 9). This decrease of Ms can be correlated to the inverse of the frequency shift and the saturation of the FWHM of the E_2^{low} mode for 15% and 20% Co substitution compared to 10% Co substitution. Therefore the additional Co concentrations ($>10\%$) are not substituting at the Zn in the ZnO host lattice. Harima *et al.*[28] have also reported phase separation at 15% Co substitution in ZnO from the Raman spectra. The substitution of Co at the Zn site was found to be proportional to the Co concentration until 10% and with a further increase of Co it preferably formed $ZnCo_2O_4$. The inset in Fig. 8 shows a hysteresis loop for $ZnCo_2O_4$ film, which is completely different than those found for the Co doped ZnO films. The $ZnCo_2O_4$ film presented a very small Ms value ($\sim 4\times10^{-4}$ μ_B/Co) and a large coercive field of $H_c \approx 5$ kOe. The magnetization results of Figs. 7 and 8 lead us to conclude that the ferromagnetic loops in our $Zn_{1-x}Co_xO$ thin films (with Co concentration up to 10%) are not due to the precipitation of any secondary phase formation of $ZnCo_2O_4$ or Co cluster in our films. Therefore, our magnetization results are in general agreement with the current interpretation that the residual impurities (Zn_i and O_v^2) act as shallow n-type donors, allowing a long-range magnetic coupling between the Co^{2+} localized magnetic moments via the conduction band.[29] The origin of room temperature ferromagnetism in DMS still remains controversial. The theoretical approach suggests that there is double exchange interaction leading to ferromagnetism in ZnCoO.[30] Park *et al.* claimed that the residual hydrogen impurities in ZnO could mediate a strong short-range ferromagnetic interaction.[31] Large concentrations of mobile carriers were not observed in high Curie temperature ZnCoO thin films reported by Yan *et al.*[32] In our case 10% Co substituted ZnO also did not show high mobile carrier concentration besides the residual impurities. To further confirm this

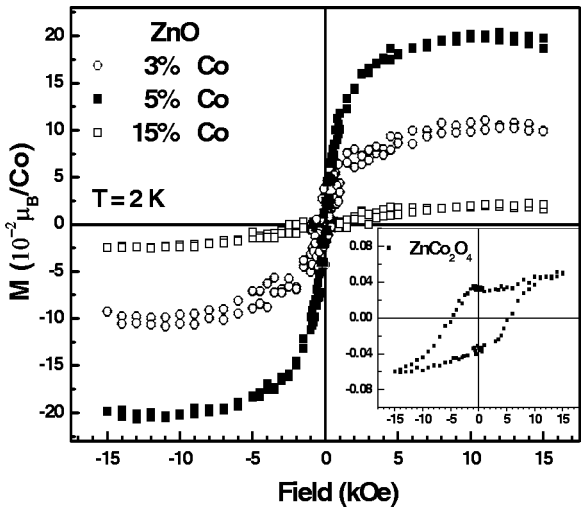

FIG. 8. Ferromagnetic hysteresis loop (M vs H) for $Zn_{1-x}Co_xO$ films (inset is for $ZnCo_2O_4$).

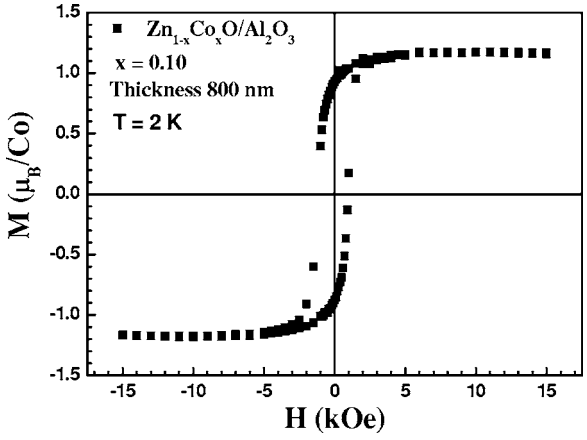

FIG. 7. Ferromagnetic hysteresis loop (M vs H) for $Zn_{0.9}Co_{0.1}O$ thin film at 2 K.

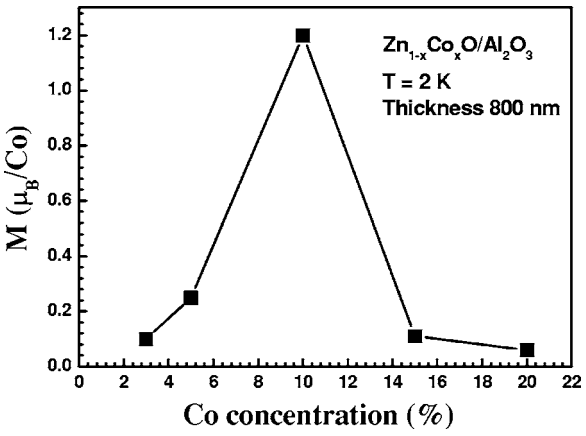

FIG. 9. Saturated magnetization at different Co concentrations at 2 K for $Zn_{1-x}Co_xO$ films.

mechanism magneto-optical and anomalous Hall effects measurements are being planned.

CONCLUSIONS

We have carried out Raman scattering and magnetic measurements on highly *c* axis oriented thin films of Co doped ZnO grown by pulsed laser deposition in our laboratory. The shift and broadening of E_2^{low} modes towards the lower frequencies were considered due to the alloy potential fluctuations, which were analyzed using a spatial correlation model and the results agreed with the experimental data. It also clearly showed that the Co ions are occupying Zn substitutional sites. The substitutions with more than 10% of Co exhibited additional Raman peaks in the spectra, suggesting the formation of the new phase, possibly $ZnCo_2O_4$. Our current studies give a unique and novel approach to establish the upper limit of uniform and homogeneous Co substitution in the ZnO lattice as compared to other techniques, which generally give a statistical average of such information. From these and the magnetic measurement data, it is concluded that the ferromagnetic (FM) properties of Co-doped ZnO are intrinsic due to the substitution of Co in the Zn lattice site of the ZnO structure. In the 10% Co substituted sample we obtained maximum saturation of magnetization, without the formation of any secondary phase. With a further increase of Co ($>10\%$) in ZnO, Raman studies clearly indicated the signature of formation of $ZnCo_2O_4$, which is antiferromagnetic in nature, and therefore, it reduced the ferromagnetic properties for concentrations over 10%.

ACKNOWLEDGMENTS

The authors acknowledge partial financial support from the Department of Defense through Grants Nos. DAAD 19-03-1-0084 and W911-NF-05-1-0304 and NASA Grant No. NCC3-1034.

[1] D. M. Bagnall, Y. Chen, Z. Zhu, T. Tao, S. Koyama, M. T. Shen, and T. Goto, Appl. Phys. Lett. **70**, 2230 (1997).
[2] S. J. Pearton, C. R. Abernathy, M. E. Overberg, G. T. Thaler, D. P. Norton, N. Theodoropoulou, A. F. Hebard, Y. D. Park, F. Ren, J. Kim, and L. A. Boatner, J. Appl. Phys. **93**, 1 (2003).
[3] D. C. Look, D. C. Reynolds, C. W. Litton, R. L. Zones, D. B. Eason, and G. Conwell, Appl. Phys. Lett. **81**, 1830 (2002).
[4] Ferromagnetism of ZnO and GaN: A review, C. Liu, F. Yun, and H. Morkoc, J. Mater. Sci.: Mater. Electron. **16**, 557 (2005).
[5] Y. Z. Yoo, T. Fukumura, Z. Jin, K. Hasegawa, M. Kawasaki, P. Ahmet, T. Chikyow, and H. Kainuma, J. Appl. Phys. **90**, 90446 (2001).
[6] M. H. Kane, K. Shalini, C. J. Summers, R. Varatharajan, J. Nause, C. R. Vestal, Z. J. Zhang, and I. T. Ferguson, J. Appl. Phys. **97**, 023906 (2005).
[7] B. Martinez, F. Sandiumenge, Ll Balcells, J. Arbiol, F. Sibieude, and C. Monty, Phys. Rev. B **72**, 165202 (2005).
[8] J. Hong and R. Q. Wu, J. Appl. Phys. **97**, 063911 (2005).
[9] T. Andrearczyk, J. Jaroszynski, G. Grabecki, T. Dietl, T. Fukumura, and M. Kawasaki, Phys. Rev. B **72**, 121309(R) (2005).
[10] T. Dietl, H. Ohno, F. Matsukura, J. Cibert, and D. Ferrand, Science **287**, 1019 (2000).
[11] K. Sato and H. Katayama-Yoshida, Jpn. J. Appl. Phys., Part 2 **39**, L555 (2000).
[12] G. P. Das, B. K. Rao, and P. Jena, Phys. Rev. B **69**, 214422 (2004).
[13] J. H. Park, M. G. Kim, H. M. Jang, S. Ryu, and Y. M. Kim, Appl. Phys. Lett. **84**, 1338 (2004).
[14] H. Fujimori, H. Komatsu, K. Ioku, S. Goto, and M. Yoshimura, Phys. Rev. B **66**, 064306 (2002).
[15] P. Parayanthal and F. H. Pollak, Phys. Rev. Lett. **52**, 1822 (1984).
[16] E. K. Koh, Y. J. Park, E. K. Kim, S. K. Min, and S. H. Choh, Phys. Rev. B **57**, 11919 (1998).
[17] J. L. Shen, I. M. Chang, Y. M. Shu, Y. F. Chen, S. Z. Chang, and S. C. Lee, Phys. Rev. B **50**, 1678 (1994).
[18] J. B. Wang, H. M. Zhong, Z. F. Li, and W. Lu, J. Appl. Phys. **97**, 086105 (2003).
[19] L. Y. Lin, C. W. Chang, W. H. Chen, Y. F. Chen, S. P. Guo, and M. C. Tamargo, Phys. Rev. B **69**, 075204 (2004).
[20] K. Samanta, P. Bhattacharya, and R. S. Katiyar, Appl. Phys. Lett. **87**, 101903 (2005).
[21] T. C. Damen, S. P. S. Porto, and B. Tell, Phys. Rev. **142**, 570 (1966).
[22] H. Richter, Z. P. Wang, and L. Ley, Solid State Commun. **39**, 625 (1981).
[23] K. K. Tiong, P. M. Amirtharaj, F. H. Pollak, and D. E. Aspnes, Appl. Phys. Lett. **44**, 122 (1984).
[24] J. Serrano, F. Widulle, A. H. Romero, A. Rubio, R. Lauck, and M. Cardona, Phys. Status Solidi B **235**, 260 (2003).
[25] F. J. Manjon, B. Mari, J. Serrano, and A. H. Romero, J. Appl. Phys. **97**, 053516 (2005).
[26] C. Bundesmann, N. Ashkenov, M. Schubert, D. Spemann, T. Butz, E. M. Kaidashev, M. Lorenz, and M. Grundmann, Appl. Phys. Lett. **83**, 1974 (2003).
[27] A. Kaschner, U. Haboeck, Martin Strassburg, Matthias Strassburg, G. Kaczmarczyk, A. Hoffmann, C. Thomsen, A. Zeuner, H. R. Alves, D. M. Hofmann, and B. K. Mayer, Appl. Phys. Lett. **80**, 1909 (2002).
[28] H. Harima, J. Phys.: Condens. Matter **16**, S5653 (2004).
[29] K. R. Kittilstved, N. S. Norberg, and D. R. Gamelin, Phys. Rev. Lett. **94**, 147209 (2005).
[30] K. Sato and H. K. Yoshida, Semicond. Sci. Technol. **17**, 367 (2002).
[31] C. H. Park and D. J. Chadi, Phys. Rev. Lett. **94**, 127204 (2005).
[32] L. Yan, C. K. Yong, and X. S. Rao, J. Appl. Phys. **96**, 508 (2004).